Biofabrication

PAPER

Valve-based consecutive bioprinting method for multimaterial tissue-like constructs with controllable interfaces

Heran Wang[1,2,3], Kai Guo[1,2], Liming Zhang[1,2], Huixuan Zhu[1,2], Shijie Li[1,2], Song Li[1,2], Feiyang Gao[1,2], Xin Liu[4], Qi Gu[4], Lianqing Liu[1,2] and Xiongfei Zheng[1,2,5]

[1] State Key Laboratory of Robotics, Shenyang Institute of Automation, Chinese Academy of Sciences, Shenyang 110016, People's Republic of China
[2] Institutes for Robotics and Intelligent Manufacturing, Chinese Academy of Sciences, Shenyang 110169, People's Republic of China
[3] University of Chinese Academy of Sciences, Beijing 100049, People's Republic of China
[4] State Key Laboratory of Membrane Biology, Institute of Zoology, Chinese Academy of Sciences, Beijing 100101, People's Republic of China
[5] Authors to whom any correspondence should be addressed.

E-mail: zhengxiongfei@sia.cn

RECEIVED
11 September 2020

REVISED
25 November 2020

ACCEPTED FOR PUBLICATION
13 January 2021

PUBLISHED
2 April 2021

Keywords: bioprinting, multimaterial construct, material interface, printing efficiency, vascularized tissue

Supplementary material for this article is available online

Abstract

Bioprinting is a promising technology focusing on tissue manufacturing, whose vital problem is the precise assembly of multiple materials. As the primary solution, the extrusion-based multi-printhead bioprinting (MPB) method requires printhead switching during the printing process, which induces inefficient motion time and material interface defects. We present a valve-based consecutive bioprinting (VCB) method to resolve these problems, containing a precise integrated switching printhead and a well-matched voxelated digital model. The rotary valve built-in the VCB printhead guarantees the precise assembling of different materials at the interface isolated from the viscoelastic inks' elastic potential energy in the cartridge. We study the coordinated control approach of the valve rotation and pressure adjustment to achieve the seamless switching, leading to a controllable multimaterial interface, including boundary and suture structure. Furthermore, we compare the VCB method and MPB method, quantitatively and comprehensively, indicating that the VCB method obtained greater mechanical strength (maximum tensile deformation increased by 44.37%) and higher printing efficiency (effective time ratio increased by 29.48%). As an exemplar, we fabricate a muscle-like tissue with a vascular tree, suture interface encapsulating C2C12, and human dermal fibroblasts (HDFB) cells, then placed it in complete medium with continuous perfusion for 5 d. Our study suggests that the VCB method is sufficient to fabricate heterogeneous tissues with complex multimaterial interfaces.

1. Introduction

In recent years, the rapid development of three-dimensional (3D) bioprinting technology has brought hope for the *in vitro* manufacture of functionalized tissues and organs, which contains typical complex multimaterial structures [1–3]. Many bioprinting methods have been applied, including inkjet [4, 5], photopolymerization [6–8], and extrusion [9–12]. The inkjet technology shows high resolution in multimaterial printing of non-biocompatible inks, but is restricted when printing higher viscosity cell-laden hydrogel. The photopolymerization bioprinting technology has the highest accuracy [13], while it confronts challenges fabricating multimaterial structure [14, 15]. At present, extrusion bioprinting is the most widely used, mainly because it is relatively easy to achieve the multimaterial distribution of biomaterial inks with a wide range of viscosity [2, 16, 17].

The primary strategy of extrusion bioprinting to deal with multimaterial problems is the multi-printhead bioprinting method (MPB) [18–21], meaning that materials are assembled outside the nozzles by switching the printheads, which brings some technical drawbacks. (a) On the one hand, the

MPB method is mechanistically incapable of avoiding defects in material switching due to the difficulty in controlling the volume and shape of each filament at the beginning and the end of each filament. Such defects form bubbles in the tissue, which affect transparency, making observation difficult, and possibly affect *in vitro* culturing adversely. Bubbles also may expand their influence layer by layer, and eventually result in a loss of overall structural accuracy. Moreover, interface tissue engineering in musculoskeletal system requires the suture structure interface [22, 23] with muscular tensile strength, no local defect, and no stress mutation. The control of such multimaterial interfaces has a significant impact on the accuracy of extrusion printing and the mechanical properties of the construct, but the control approach has rarely been reported. (b) On the other hand, from the technical implementation perspective, the multi-printhead method takes an immense amount of non-efficient time on the switching of printheads, the calibrate of nozzle positions, and the deceleration of motion adjustment; therefore, it is challenging to guarantee the production efficiency with controlled manufacturing time, which is crucial for cell activity and experiment repeatability.

These challenges should be resolved by breakthroughs in two aspects: Printing process and printhead design, and digital model for interface control. (a) Printing process and printhead design. Some exciting studies about continuous multimaterial extrusion were conducted [24–26], indicating continuous cell printing feasibility. Considerable research about the 3D printing method based on the confluent nozzle was carried out [27], demonstrating the possibility of the high resolution of soft matter printing. Even so, the high viscoelasticity of biomaterials leads to a slow release of the elastic potential energy within the material during the actual printing process, resulting in a large error between the actual output and the input control signal, which significant represented by the interface [22] formed between switched materials. This problem also causes the current one-nozzle multimaterial printing to avoid the start and stop of ink, which is also equivalent to the interface between the ink and air. However, this problem has rarely been mentioned or researched, and even fewer printhead design solutions have been proposed to address it. (b) Digital model for multimaterial interface control. At present, the bioprinting software mainly uses the method of industrial 3D printing as reference, which needs to be improved urgently. When it comes to industrial production, only the external surface quality of uniform material parts is generally concerned, while bioprinting focuses on the internal structure of tissues and the distribution of multiple materials. There has been a great attempt in the inkjet 3D printing field to integrate multiple data sources into a single voxel digital model [28], providing a reference for bioprinting. A digital model is urgently in demand, where multidimensional information can be stored and manipulated, including geometry, material, interface, and control information. The digital model and its software-based workflow should have sound versatility and extensibility for its being an essential basis of various biological manufacturing technologies.

In this work, we present a valve-based consecutive bioprinting (VCB) technique for fabricating multimaterial tissue-like constructs with controllable interfaces. Firstly, we designed an innovative printhead in which the rotary valve isolates the biomaterial ink [29] elastic potential energy from a precision interface assembling to achieve rapid and seamless switching and neat pre-assembly of multiple materials. For this process, we developed a digital model and a software workflow both with extensibility and flexibility. We then demonstrated the control method and the applicability for the interface tissue engineering manufacturing and made a comprehensive and quantitative comparison between the VCB method and the MPB method. Finally, the manufacture, perfusion, and culture of a muscle-like tissue with vascular tree, C2C12, and HDFB cells were performed to verify the effectiveness of the VCB method. We anticipate that the VCB method could be widely used in bioprinting to produce multimaterial tissues and organs.

2. Materials and methods

2.1. Bioprinter

The bioprinter (SIA bioprinter PRO) was designed and manufactured by our research team, upgraded based on the SIA bioprinter LITE [30] and SIA bioprinter PRO initial generation [31]. The bioprinter (figure S1(a), supporting information (available online at stacks.iop.org/BF/13/035001/mmedia)) includes precision motion control function (triaxial positioning accuracy ± 5 μm), temperature control function (± 0.1 °C), and modular interface that can be adapted to various types of nozzles, including ordinary independent printhead for multi-printhead printing process and specially designed integrated printhead for VCB process. The size range of the printing head nozzle is suitable for 50 μm–400 μm; the pressure adjustment range is 0.1–600 kPa; the temperature control element adopts semiconductor chip; the temperature control range is -4 °C–40 °C; and the bioprinter can achieve extrusion, ink-jet, and light curing.

2.2. Design of printhead

The consecutive printhead (figures S1(b) and (c), supporting information) was designed to consist mainly of six parts: an interlaced valve, a confluent nozzle, a channel distributor, three ink cartridges, two temperature control zones, and three independently

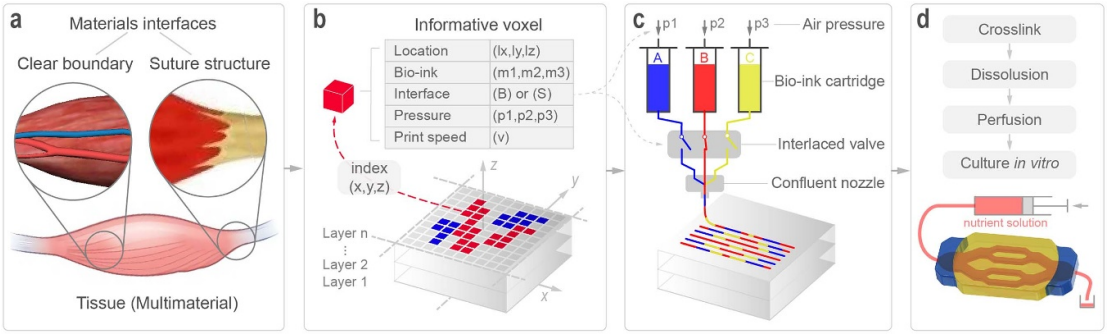

Figure 1. Schematic diagram of the valve-based consecutive bioprinting (VCB) process. (a) Tissue structure model analysis and reconstruction, including two types of material interfaces (clear boundary and suture structure). (b) Informative voxelated digital model integrated from the geometrical model with multidimensional information, including location, biomaterial ink, interface, pressure, and speed. (c) Principle of the consecutive print. Printhead primarily composed of an interlaced valve and confluent nozzle and controlled by signals calculated from the model. (d) Post-processing for culture *in vitro*, containing crosslink of body material, dissolution of sacrificial material, and culture medium perfusion.

controlled air pressures (figure 1(c)). The signals from the digital model (figure 1(b)) can simultaneously control the valve rotation, the pressure valve, and the nozzle position.

The interlaced valve was designed to contain a rotatable core and a static jacket, with three inlets and three outlets, ground from biological zirconia ceramics. The three channels' distributional circle diameters $d1 = 3.0$ mm, $d2 = 6.4$ mm, and $d3 = 9.8$ mm, respectivelyshown in figure 2(b). As the channel diameter in the core part was 1.0 mm (1.2 mm in the jacket), different channels could never have overlap; the nearest distance was 1.4 mm, for the cyan channel was 30° inclined, and the long axis was 2.0 mm. To guarantee the valve's leakproofness, the interval between the core and jacket was 8 ± 2 μm, and the tangent surface roughness *Ra* was less than 0.4. Driven by a DC servo motor (24 V, 250 r min^{-1}), the valve core completed the switching rotation (120°) in 80 ± 10 ms.

The confluent nozzle was made by stainless steel (AISI 316L) to keep the roundness of the channels. The diameters of the three channels and the terminal channel were uniformly set to 150 ± 10 μm. The intersection angle between channels was decided to be 120°. The tip of the nozzle was specially designed with a smooth arc surface, conducive to the bonding and levelling of the structure when bioprinting.

In the channel distributor (photoconductive ABS), the diameters of three channels were 1.3 mm, 1.5 mm, 1.7 mm, respectively, according to the principle of equal flow resistance (figure S1(c), supporting information).

The printhead contained two independent temperature control zones: the cartridge, and the nozzle (control accuracy: ±0.1 °C), realized by semiconductors (Semiconductor model (TES), 24 V, 3 A for cartridge and 6 V, 2 A for nozzle), a fluid-cooled heat sink (6061 aluminum alloy) and self-designed PID controller.

The three air pressures were controlled by the electric proportional valves (SMC, ITV0030-OML), with a control accuracy of ±6% and hysteresis of ±0.5%.

2.3. Digital model and algorithm

MATLAB (version: 2020a) was utilized to implement the whole digital model construction and the process algorithm design (figure S2, supporting information). The original data sources could be 2D images (.jpg, .png, *et al*), solid geometry (.stl), or even quantitative physiological principles (equations). They would be integrated into an informative voxel digital model, stored in a multidimensional array. The voxel size (*x*/*y* direction) was defined as 150 μm depend on the diameter of the printhead nozzle.

The data of each layer was regarded as a digital picture, which was applied to image processing algorithm (MATLAB image processing toolbox) to realize the structural design and control planning, including (a) design algorithm of area, (b) coordinated equations of anatomy, (c) structure design of pore, (d) control setting of interfaces, and (5) planning algorithm of traces. To increase computation speed, the matrix programming method was applied when dealing with large-scale matrix operations.

2.4. Biomaterial inks

Pluronic F127 [18] (Sigma-Aldrich, USA, final concentration 20% w/w, 25% w/w, 30% w/w) was dissolved in deionized water containing 1.5% w/v pigment. Photocrosslinkable Pluronic F127 was synthesized using a previous method [32] and dissolved in deionized water without pigment with a final concentration of 25% w/w.

Polyethylene glycol diacrylate (PEGDA) was synthesized as described previously [6]. Briefly, 5.0 g PEG (10 kd Sigma-Aldrich, USA) was dissolved in 15 ml anhydrous dichloromethane followed by the addition of 0.44 ml methacrylic anhydride (Sigma-Aldrich, USA), 0.25 ml trimethylamine, and 3 g

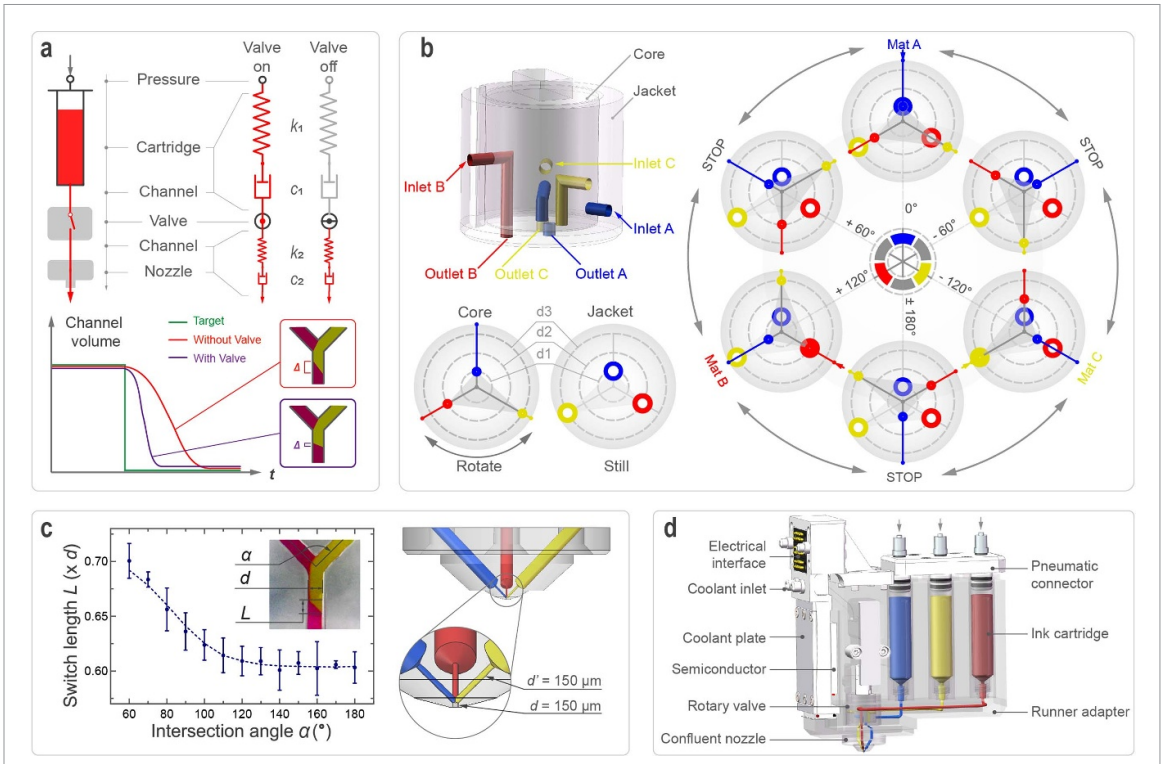

Figure 2. Design of the VCB printhead. (a) Schematic of the terminal valve. At the printhead terminal, the valve isolates the elastic potential energy stored in the viscoelastic material, facilitating precise and rapid switching control. (b) Constitution of the interlaced valve containing a core and a jacket with three inlets and three outlets and distribution of channels on different diameters. Rapid switching and On–off control method diagram of three materials. The experiment was performed in a microfluidic chip (Pluronic F127 with pigment). (c) Relationship between the intersection angle of channels and switching length of two materials and structure of the confluent nozzle with 150 μm diameter. (d) VCB printhead structure diagram.

molecular sieves. After thoroughly mixing, the solution was allowed to react for 7 d at room temperature in the dark. The final PEGDA suspension was dried overnight under high vacuum with a cold trap until completely dry. The dried PEGDA was then dissolved in H_2O at 20% concentration (w/v) and dialyzed against H_2O to remove all low-molecular-weight molecules using 3000 NMWCO dialysis sacks.

Biocompatible nanoclay (Laponite XLG, BYK Additives, Inc., TX, USA, final concentration 6% w/v) was dissolved into deionized water containing 0.15% w/v photoinitiator lithium phenyl-2, 4, 6-trimethylbenzoylphosphinate (Sigma-Aldrich) and 1.5% w/v pigment, 10% or 20% w/v of PEGDA until forming a stable hydrogel, allowed all the ingredients to homogenize and settled overnight in the dark.

2.5. Rheological test

The materials used in this paper were subjected to rheological tests (Model of rheometer (RST-CPS) cone plate rheometer, Brookfield, AMETEK, USA). The type of spindle used in the test is RPT-25 (viscosity measurement range is 0.03–2.49 MPa s^{-1}). The relation curve between shear rate and shear stress was measured by shear stress scanning mode, and the shear stress increased from 0 to 1000 Pa (under low shear stress, the shear rate was very small, even less than the noise of the signal, so it was ignored when used to identify the parameters of the material model. The plot of shear force versus shear rate was in the range of 367 Pa–1000 Pa). The viscosity and shear rate curve is obtained by shear rate scanning, and the scanning range is 2×10^{-2}–2×10^{2} s^{-1}. Rheometer standard yield stress test procedure was used for the measurement of yield stress. For the tests of dynamic modulus G′ and G″, we used MCR 302 rheometer (Anton Paar, USA), parallel plate probe model PP25, and the frequency sweep range was 1×10^{-2}–1×10^{2} s^{-1}.

2.6. Control preparation of VCB

To ensure the VCB control effect, four progressive steps are carefully conducted: (a) discrete micro-dots printing. The reference pressures (accurate to 1 kPa) of three channels were adjusted precisely to guarantee the extrusion volume is nearly equal (less than 5% error, by image process) during the same period. (b) On–off control. A line segment model with an interval greater than 0.5 mm was used to verify the On–off performance on a complete track. (c) Consecutive interface control. For boundary, 180 Pa regulation was achieved at a distance of 1 voxel (150 μm), while for suture, 60 Pa regulation was achieved at a distance of 2 voxels (300 μm). For different materials, the pressure values were different; thus, the adjustment should be prepared before printing. (d) Switching delay compensation. For ease of measurement, print experiments with serpentine trajectories were

carried out to double the delay distance. For example, the difference of 0.26 mm reflects a delay of 0.13 mm.

2.7. Printing process

The parameters used in VCB were as follows: printing speed 20 mm s^{-1}, layer height 150 μm, filament space 180 μm, printhead temperature 25.0 °C, print plate microscope slides (Titan Scientific, China). The procedures for the aseptic operation were as follows: (a) turn on UV sterilization for 20 min before bioprinting; (b) soak the inside channels of the printhead with 75% alcohol for 30 min; (c) keep the HEPA filter of bioprinter open before and during printing.

2.8. Tests of printed constructs

In order to quantitatively analyze the effect of material switching, for both the VCB and MPB method, an image processing analysis algorithm was designed. The printed constructs' size was 20 × 10 × 1 mm^3, with the material boundary in the middle and filament spacing less than 0.2 mm. Photos taken directly above were taken screenshots of the central area (18 × 8 mm^2), under the consistent light. The images were converted into grayscales, and the grayscale value was taken as the average value of each column, and then the low-pass filtering was performed to obtain the quantized material distribution value.

To assess the mechanical properties of the printed constructs with material interfaces, for both the VCB and MPB method, tensile modulus tests were carried out. The length, width, and height of the samples were 20 mm, 4 mm, and 2 mm, respectively. Five groups of samples had different filament space values: 0.15 mm, 0.2 mm, 0.25 mm, 0.3 mm, 0.35 mm. The layer height was 150 μm, and the filament diameter was ~180 μm, which means that the filaments separate under large space. The tensile tests were carried out by texture analyzer (CT3-100, Brookfield, AMETEK, USA) with a self-designed fixture. The clamps were fixed on the upper and lower ends of the analyzer; the two ends of the test specimen were glued to two plastic sheets, and the analyzer was set to gradually elongate at a rate of 5 mm s^{-1}, which is equivalent to a strain rate of 0.25 s^{-1}; the tensile length was recorded with a stress drop of 5% as a tensile break, and divided it by the original length of 20 mm, which was the maximum relative tensile deformation.

To assess the structural defects caused by material switching, for both the VCB and MPB method, the transparency detection tests were carried out. The samples (20 × 20 × 2 mm^3) were printed by Pluronic F127 (25% w/w) without pigments at 25.0 °C. The data obtained by the light transmittance tester (LH-206, Puyan) was limited to visible light.

The 3D images of printed microstructures were obtained by a light-sheet microscope (Luxendo MuVi CS, Bruker Corpo-ration). The parameters were set as follows: 561 nm laser, power 10%, emission filter LP572, imaging lens 10×/0.5, changing times 0.75×, lighting 10×/0.3 object lens, exposure time 20 ms, height (X) imaging range 11.6 mm (view step 1.16 mm), width (Y) imaging range 5.8 mm (view step 1.16 mm), depth (Z) imaging range 4.5 mm (view step 10 μm).

2.9. Cell culture

Human dermal fibroblasts (HDFB, ScienCell, USA) and C2C12 (ATCC, USA) were cultured in Dulbecco's modified Eagle medium containing high glucose (Gibico, Invitrogen, USA) and supplemented with 10% fetal bovine serum FBS (Gibico, Invitrogen, USA), 100 units ml^{-1} penicillin, and streptomycin (Gibico, Invitrogen, USA).

2.10. Cell maintenance and staining

HDFB and C2C12 were labeled blue and red fluorescence using live cell labeling kits (PKH26 red fluorescent cell linker kit for general cell membrane labeling, Sigma-Aldrich, and CellTracker™ blue CMAC dye, Thermo Fisher Scientific, USA). Carefully mixed the material and cell suspension using a double mother Luer connector. The concentration of cells after mixing cells and material was 5 × 10^5 cells ml^{-1}. The Viability/Cytotoxicity Kit (Thermo Fisher Scientific, USA) was used to examine the post-fabrication cell viability by epifluorescence microscopy after 1 and 5 d. Cell-laden hydrogels were washed with D-PBS twice; subsequently, a diluted LIVE/DEAD staining solution was added to the hydrogel for 60 min. Fluorescent microscope was used to image the stained gels. Three hydrogel images were taken, and the number of live and dead cells was counted per image. The percent of live cells determined cell viability over the total cell counts. Software ImageJ was used to quantify the live and dead cell numbers.

3. Results

3.1. Valve-based consecutive printhead

Herein, we designed a printhead with a novel structure (figure 1(c)). On the one hand, we used an interlaced valve for rapid and precise switching of multiple materials. On the other hand, we used a confluent nozzle for preassembled and accurate extrusion of multiple materials. Thus, this specially designed printhead is suitable for the consecutive fabrication of multimaterial structures. According to the Maxwell model, viscoelastic biomaterials can be regarded as an elastic unit in series with a viscous unit (figure 2(a)). In the printhead, the large cartridge and the long channel will store much elastic potential energy. Meanwhile, the channel and nozzle behind the valve are small in size, thus having the little elasticity and viscosity. When the material is switched, the elastic compression within the material is only slowly released due to viscous influences, which leads to an

increase in the control error of the extruded volume, making precise control difficult. The rotary valve at the end of the flow path isolates a large volume of material by rotating instantaneously, thus reducing the viscoelastic influence and improving the control accuracy of the multimaterial interface.

To meet bioprinting requirements, we chose the form of a rotary valve rather than the traditional needle valve. For the rotary valve, the channel volume remains unchanged during the motion, resulting in a stable fluidic pressure (figure S3, supporting information), which is advantageous for controlling accuracy and cell activity. The valve contained two components: the rotatable core and the static jacket, with three inlets and three outlets in an interlaced manner (figure 2(b)). Moreover, we skillfully designed the flow channel distribution (figure 2(b)) to realize the rapid switching and On–off control of three materials (figure 2(c)). For example, when the valve core turns to 0°, only channel A will be unblocked, so that the material A will be extruded by the air pressure specially set. If the material extrusion needs to be stopped, the valve core will turn to 60° or −60° (decided by the next material), where all the channels are blocked. Driven by a DC servo motor, the valve core completed the switching rotation (120°) in 80 ± 10 ms. Furthermore, since the channel diameter covered only 11.5° of the circle, it only takes ~8 ms for a channel from on to off (60°). Also, by the particular design of the flow path distribution, the rotary valve can be cleverly designed so that the flow path of each material is entirely free from contact with the other flow paths, structurally avoiding contamination between materials.

To improve the material switching effect, we studied the influence of the intersection angle of channels α on the material switching length L (figure 2(d)): L decreased as α increases from 60° to 180° with indistinctive effect. Besides, considering that the shorter terminal channel allows for less delay, we designed a confluent nozzle with 150 μm diameter and 120° intersection angle (figure 2(d)).

Based on the interlaced valve control and the confluent nozzle structure, the printhead (figures 1(d) and S1(b), supporting information) achieved consecutive extrusion of multiple materials from one nozzle (movie S1, supporting information), which could be named as VCB technology.

3.2. Voxelated digital model

We proposed a novel bioprinting digital model and software architecture matching the demand for precision multiple materials' switching in the VCB method (figure 1(b)), which is more extendible and flexible than traditional ways. In this workflow, the original data sources, including 2D images, solid geometry, or even physiological principles, will be discredited and integrated into an informative voxel digital model, neatly stored in a multidimensional array (figure S2, supporting information). In this paper's specific application, the discrete size in x/y direction was set as 150 μm based on the diameter of the nozzle. Every independent voxel, located by a unique index vector, contains all the needed information: location, biomaterial ink, interface, pressure, and speed.

This voxelated digital model provided an extensible and flexible method not only for data input but also for the digital process afterward. The data of each layer could be regarded as a digital picture, which can be applied to image processing algorithm for the structural design and control planning, including design algorithm of area, coordinated equations of anatomy, structure design of pore, multimaterial printing mode setting, and planning algorithm of traces (figure S2, supporting information).

3.3. Control method of VCB

We conducted control tests for the valve-based consecutive printhead and voxelated digital model (figure 3). We utilized Pluronic F127, which is easy to formulate, rheology stable, and is a typical Herschel–Bulkley (H-B) fluid, making it convenient as an alternative ink for testing [18]. We tested the rheological profile of F127 (25% w/w) at the temperature of 25.0 °C and fitted it using the H-B model, which proved that the material is consistent with the H-B model. Besides, we also compared the fit of the H-B model with the power-law model for F127 (figure S4(a), supporting information), and the results show that the H-B model is more relevant to the experimental data. H-B fluid is a fluid widely used in bioprinting [25, 27], which can maintain a stable shape when the force is less than the yield stress.

Based on past experiments, inks that conform to the H-B model are mostly printable. Moreover, the rheological property could be neatly controlled by the concentration (figures 3(b) and (c)). With the inks ready, we performed a five-step control test (figures 3(c)–(f)). (a) Firstly, three channels' reference pressures were adjusted precisely to guarantee the extrusion volume is nearly equal (diameter 376, 390, 375 μm on average, less than 4% difference) during the same period, through the discrete micro-dots printing test (figure 3(c)). The three channels' reference pressures are determined as 200, 242, 288 kPa respectively correspond to ink with cyan, magenta, yellow pigment, resulting in the dot diameter of 386 ± 19 μm during the motion pause of 200 ± 10 ms. The difference in pressure value mainly comes from the asymmetry of the channel structure. (b) Secondly, after adjusting the pressure, we carried out the On–off control test to verify the control logic and rotate function of the interlaced valve (figure 3(e)). Herein, the character pattern 'SIA' was printed, showing clear starting and ending points of filaments. We used the image processing method to obtain the boundary of each filament and count the filament widths, and the

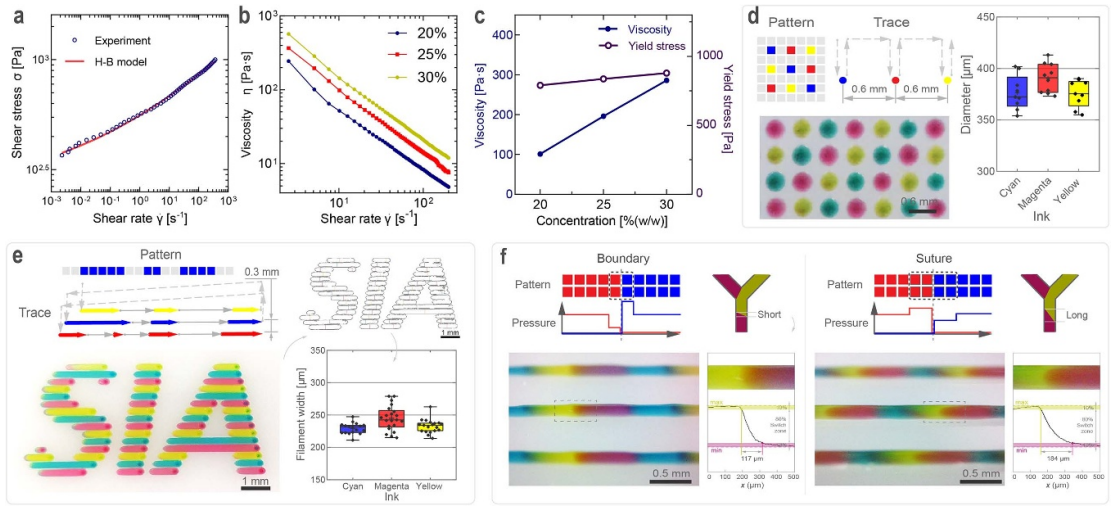

Figure 3. VCB control method utilizing Pluronic F127 with pigment. (a) Plot of shear force versus shear rate for Pluronic F127 (25% w/w), and fitted H-B model curves. (b) Rheological flow curves of F127 (20%, 25%, 30% w/w), showing the property of thinning shear and the effect of different concentrations on viscosity. (c) Rheological property control curve based on concentration regulation where the viscosity is taken uniformly at a shear rate of 5.0 s^{-1}. (d) Reference pressure adjustment process by printing the discrete dot matrix (diameter 376, 390, 375 μm on average, less than 4% difference). (e) On–off control test on the character pattern of 'SIA'. The image processing method was used to obtain the boundary of each filament and count the filament widths, and the results show that the average filament widths of the three materials are 229 μm, 245 μm, 233 μm. (f) Consecutive interface control test in a single filament, facing the requirements of boundary interface (short bevel in nozzle) and suture interface (long bevel in nozzle), respectively. The coordinated control approach of the valve rotation and pressure adjustment was able to actualize the material pre-assembly and seamless switching. In the image processing, 10% of the difference between the maximum and minimum values of the curve is taken as the unmixed region, while the middle 80% of the transition is defined as the actual switching length of the material, thus quantifying the material switching lengths of 117 μm and 184 μm for both approaches.

results show that the average filament widths of the three materials are 229 μm, 245 μm, 233 μm. (c) Thirdly, we conducted the consecutive interface control test containing two type interfaces [22]: boundary and suture (figure 3(f)). Boundary represents a distinct interface between materials (muscles and blood vessels), while suture represents a continuous interleaved structure between materials (muscles and tendons) [23]. In that case, we set different pressure adjustment values for voxels at different interfaces: ±180 Pa for boundary and ±60 Pa for suture. From the print image of a single filament, the control method based on the coordination of the valve and pressure was feasible. In the image processing, 10% of the difference between the maximum and minimum values of the curve is taken as the unmixed region, while the middle 80% of the transition is defined as the actual switching length of the material, thus quantifying the material switching lengths of 117 μm and 184 μm for both approaches. (d) Moreover, we tested and compensated the switching delay (figure S2, supporting information) caused by the material joint zone in the nozzle (figure 2(e)). Experimentally, the delay distance was measured as ~0.13 mm, which equaled half of 0.26 mm because one circulation could double the delay. Therefore, we advanced the control parameters by 1 voxel (=150 μm) in the software. In summary, this four-step control test demonstrated the controllability and flexibility of the VCB method and laid the foundation for practical application. (e) Finally, we analyzed the printed constructs' switching speed by designed image analysis software (figure S6, supporting information). This innovative, detailed control approach provided a vital foundation for the VCB method.

3.4. Manufacture of muscle-like construct

In this study, we fabricated a muscle-like construct with serrated suture (figure 4) to verify the VCB method's adaptability to different inks and consecutive multibody. For example, particular muscle tissue is bonded by muscle belly tissue and tendon tissue (figure 1(a)), which have a considerable difference in modulus but an interface with robust mechanical properties. The suture [23], as a typical bionic structure, could enhance the interface bonding strength between different materials [33]. Interestingly, because the materials are preassembled with an angle in the nozzle (figure 2(e)), the VCB method could be natural and suitable for forming the suture structures (figure 3(e)).

Herein, we designed a multibody structure consisting of five bodies, connected by suture structures, using cyan and yellow to represent different materials. (figure 4(a)). The cyan part contained 20% PEGDA (molecular weight 10 000), 6% biocompatible nanoclay (Laponite XLG, BYK Additives, Inc., TX, USA) and 1.5% cyan pigment; while the yellow part contained 10% PEGDA, 6% biocompatible nanoclay and 1.5% yellow pigment. Nanoclay was also proved to be a fluid that conforms to the H-B model (figure S4(b)). The dynamic rheological test curves of the

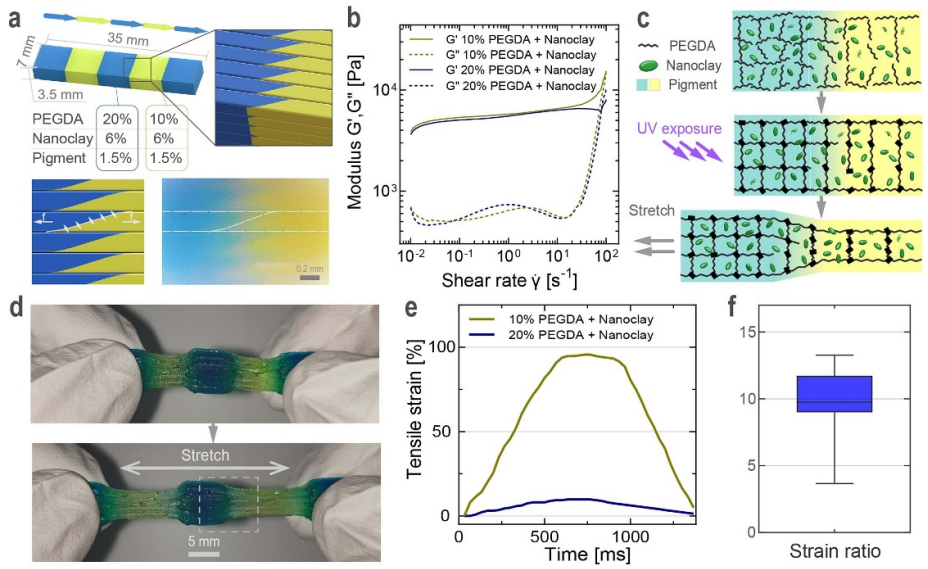

Figure 4. Design, print, and test of a muscle-like structure with a suture interface between materials. (a) Design and print of the muscle-like consecutive multibody with a suture interface. The cyan part simulated tendon tissue with 20% PEGDA and 6% nanoclay and the yellow part simulated muscle belly with 10% PEGDA and 6% nanoclay. (b) Dynamic modulus test curves of the two materials show that the rheological properties of the two materials are very similar. (c) Mechanism of the solidification and the deformation of the consecutive multibody material. The VCB method can realize the pre-assembly of multiple materials in the nozzle, and then the light solidification is achieved outside the nozzle, resulting in a robust and well-fused material suture interface. (d) Qualitative tensile test of the printed muscular-like structure. (e) Tensile strain diagrams for both material regions were obtained by intercepting a video of 1.4 s duration and performing image recognition. (f) The multiplicative relationship between the tensile strains of the materials also reflects the modulus relationship between the two materials, averaging a 9.98-fold difference between the two materials.

two materials (figure 4(b)) showed that they have similar rheological properties, reflecting the fact that clay plays a significant role, while different concentrations of PEGDA have less influence on the rheological properties.

Figure 4(c) demonstrated the solidification mechanism and the deformation of the consecutive multibody material, especially the interface part. After UV light polymerization, the different concentrations of PEGDA will lead to different elasticity modulus, and because the connection part got a consecutive concentration gradient, it can form a streamlined shape with superior mechanical strength. We carried out the tensile test on the printed construct, showing admirable connection strength and stretching and spring-back behavior similar to muscle tissue, intuitively (movie S2, supporting information). The tensile strain in the region of the two materials (figure 4(e)), where the strain is obtained by dividing the deformation value by the initial size, is shown by intercepting 1.4 s in the video and performing image recognition, which reflects the significant difference in modulus between the two materials. More clearly, we counted the ratio of strain per frame, which also reflects the ratio of modulus, and the results show that the average difference in strain or modulus between the two materials is 9.98 times. As a natural feature of the VCB method, the materials are preassembled inside the nozzle, extruded continuously, and solidified outside the nozzle to form a robust and well-fused material suture interface. Therefore, VCB provides a solution for the construction of consecutive multimaterial tissue with high-stress transfer requirements.

We conducted a quantitative comparative study on VCB and MPB methods in four aspects (figure 5). (a) To characterize the structural defects caused by material switching, we carried out the transparency detection (figure S8, supporting information) because the scattering of light can reflect the material heterogeneity and the bubbles inside. When using the MPB method, the printed matter often has many bubbles, resulting in poor overall light transparency. Therefore, the higher the interface accuracy, the fewer defects and the higher the transparency of the printed tissue. We use the physical quantity of light transparency to quantitatively compare the relative accuracy of the interface of different printing methods. The results showed that the VCB method's transparency was 5.5% higher than that of the MPB method. (b) To study the mechanical properties of the constructs manufactured by different methods, we performed five groups of maximum elongation tensile tests (figure 5(b)). Interestingly, the two methods showed significant distinction for different printed constructs: the test constructs of the VCB method showed remarkable data stability and high tensile strength (mean: 264.2%), while the MPB method sometimes results in low mechanical properties (minimum: 72.0%), indicating that the VCB method obtained higher mechanical strength up to 44.37% on average. The maximum tensile deformation reflects the maximum stress that the printed

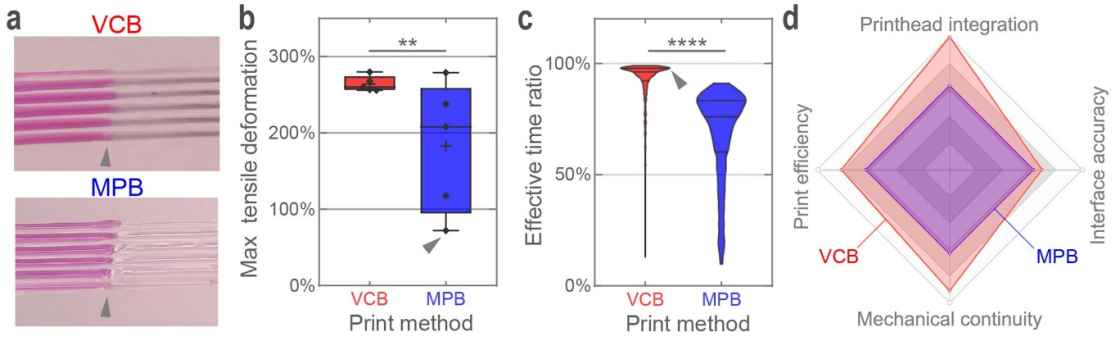

Figure 5. Comprehensive comparison of VCB and MPB (multi-printhead bioprinting). (a) Image of single filament F127 (25%) printing experiment. The MPB method caused apparent defects at the material interface, but VCB method realized multimaterial filaments with a uniform diameter. (b) Box-and-whiskers diagram showing all maximum tensile deformation of printed sample (mean: 264.2% and 183.0%, minimum to maximum, $**p < 0.05$, $n = 5$). (c) Violin plot of effective time ratio of 500 simulations each method ($****p < 0.0001$, $n = 500$). (d) Spider map of the method comparison in four dimensions: interface accuracy (by transparency), mechanical continuity (by tensile deformation), print efficiency (by effective time ratio), and printhead integration (by the number of materials a printhead can handle per unit mass).

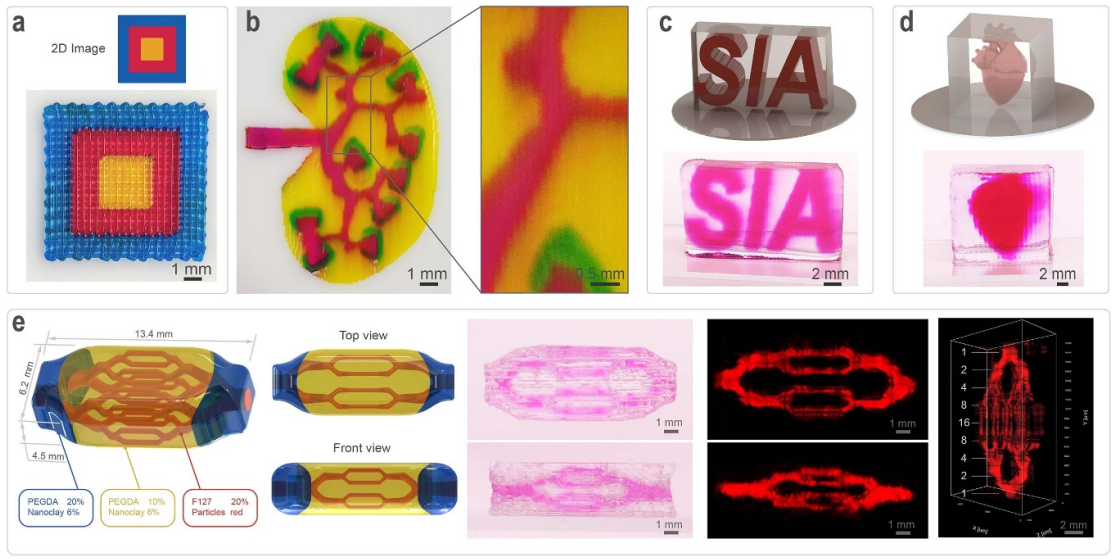

Figure 6. Print test images of VCB method. (a) Continuous multibody mesh structure. (b) Metanephroi-like multimaterial structure. (c) Stereoscopic text 'SIA'. (d) Heart-shaped 3D structure. (e) Design drawings, physical photographs, and confocal images of the muscle-like construct ($13.4 \times 6.2 \times 4.5$ mm^3) containing 16 branches of blood vessels by Photocrosslinkble Pluronic F127 (25% w/w).

matter can withstand before it breaks, so it can be used to characterize the strength of the printed matter's multimaterial interface and the overall mechanical continuity. (c) To assess the time efficiency of different printing methods, we ran 500 simulations and recorded the effective time ratio (figures 5(c) and S9, supporting information). The effective time ratio is the rate of the effective time to the total time during the entire printing process, where effective time is the time spent on extrusion. This parameter provides a quantitative characterization of the time utilization, which indicates the printing efficiency of different printing methods. On average, the VCB method was 29.48% more efficient than the MPB method because VCB could eliminate the additional time, such as the switch of printheads, the calibrate of nozzle positions, and the deceleration of motion adjustment. (d) Finally, we innovatively designed an indicator to measure the printhead's integration, which equals the number of materials a printhead can handle per unit mass. For our current printhead design, the VCB printhead is 58% more integrated than MPB. To sum up, due to different mechanisms, the VCB method had apparent advantages over the MPB method in many aspects: interface accuracy, mechanical continuity, print efficiency, and printhead integration (figure 5(d)).

3.5. Printing tests of VCB method

To verify the printing effect of the VCB method, we carried out a series of printing tests. Firstly, we printed a continuous multibody mesh structure (figure 6(a)), demonstrating the notable material switching ability. We then printed a metanephros-like

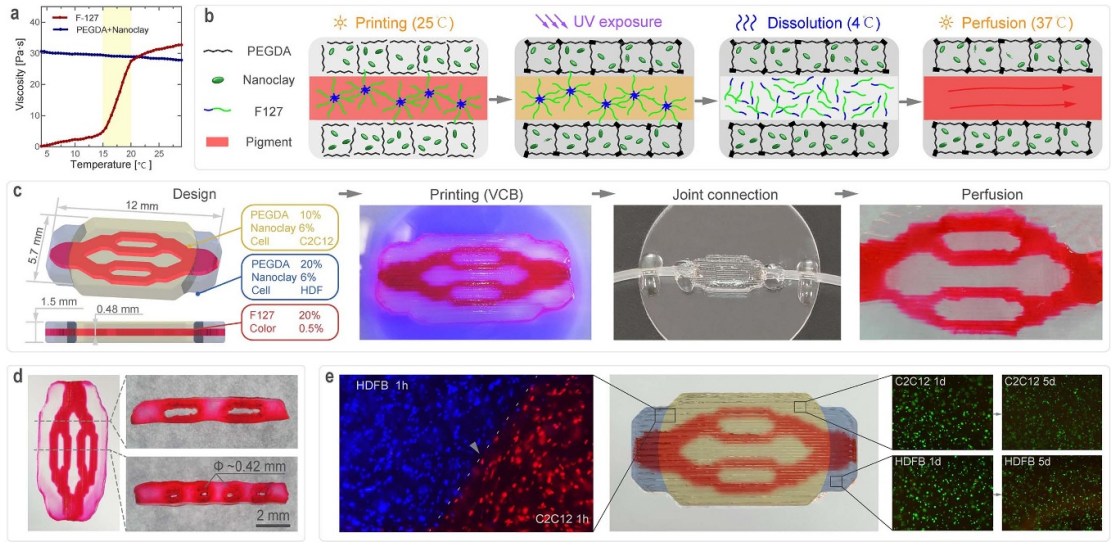

Figure 7. Design, printing, perfusion, culture, and test of a muscle-like tissue containing a network of blood vessels and multi-cell interface. (a) Viscosity of two materials varies according to temperature. The yellow area indicates the temperature region of the property transition of F127, where the viscosity changes dramatically with temperature. The left side of the region is considered fluid and the right side is considered solid. (b) Mechanism of material solidification and vascular formation. (c) Whole process of manufacture and culture of the tissue. (d) Cross-sectional images of vessel structure for 5 d culture. (e) Image of multi-cell interface and fluorescent image of LIVE/DEAD (green/red) cell viability stains of C2C12 and HDFB at 1 and 5 d.

multimaterial structure (figure 6(b)), indicating the ability to print micro heterogeneous structures with a 100 micron resolution. Moreover, we carried out large volume 3D structure printing, including the stereoscopic text 'SIA' (figure 6(c)) and heart-shaped 3D structure (figure 6(d)), demonstrating the excellent transparency achieved by the VCB method. Finally, we manufactured the muscle-like construct ($13.4 \times 6.2 \times 4.5$ mm^3) containing 16 branches of blood vessels (figure 6(e)). The 3D vascular network was designed as a five-stage network with branching mode '1-2-4-8-16-8-4-2-1', and the smallest vessel diameter was 0.36 mm. Besides physical photographs, the light-sheet microscope image and video also demonstrated the VCB method's ability to print tiny tissue with a complex vascular tree (movie S3, supporting information).

3.6. Manufacture of muscle tissue with vascular tree

According to the different temperature-sensitive (figure 7(a)) and photosensitive properties of Pluronic F127 [18] and PEGDA/nanoclay, we designed a fabrication process of muscle tissue with a vascular tree based on VCB technology. In this process, all the materials were printed simultaneously, whereas only cell-laden PEGDA/nanoclay was cross-linked by UV light (figure 7(b)). The vessel part is occupied by solid-state Pluronic F127 at 25.0 °C, which will be dissolved and douched at 4.0 °C as the sacrificed material [9] and form a cavity vascular network [1].

The designed construct consisted of three parts (figure 7(c)): (a) the muscle belly (yellow part) consisted of PEGDA (10% w/v), nanoclay (6% w/v) and C2C12 (1×10^6 cells ml^{-1}); (b) the tendon (blue part) consisted of PEGDA (20% w/v), nanoclay (6% w/v) and HDFB (1×10^6 cells ml^{-1}); (3) the blood vessels (red part) consists of Pluronic F127 (20% w/w) and fuchsia food color (0.5% v/v). The vascular tree was designed as a three-stage network with branching mode '1-2-4-2-1', where the thickness of vessels at all stages was 0.48 mm, while the width of vessels is different, respectively 0.48, 0.96, and 1.92 mm. At the inlet and outlet ends, we also designed a noose structure (width 0.64 mm) to ensure a seal between the vessel and the joint.

After the VCB method printing (movie S4, supporting information), the printed tissue was solidified by the UV radiation (10^{15} mW cm^{-2}, 5 min). The tissue was then placed in 4.0 °C ultra-pure water for 10 min until the Pluronic F127 was dissolved and diffused out. Next, the printed tissue vessels were connected to the silicone tubes, using the PEGDA to ensure the seal. The printed tissue was perfused using PBS solution mixed with food color (2% v/v, tulip red, AmeriColor Corp, Soft Gel Paste) for exhibition (movie S5, supporting information). We used a culture medium (2 ml h^{-1}) to instill the printed tissue for 5 d.

The tissue was sectioned after 5 d of culture (figure 7(d)), suggesting good shape retention of the vascular structure. The interface between HDFB (blue labeled) and C2C12 (red labeled) was obvious 1 h after printing (figure 7(e)), reflecting the interface control ability of VCB when printing cells. The viability of C2C12 and HDFB was 92 ± 1.8% and 90 ± 1.2% after one day culturing, 84 ± 2.7%, and 82 ± 2.9% after 5 d culturing. The reduction in viability between day 1 and 5 is significant ($p < 0.05$,

$n = 3$), mainly because the blood vessel network is not dense enough, the nutrition and oxygen cannot meet the needs of cells. This speculation is based on the phenomenon observed in our experiments: the survival rate of some cells close to the blood vessel is high, while the survival rate of some cells far away from the blood vessel is low.

4. Discussion

At present, multimaterial bioprinting is considered an essential means for constructing complex tissue, especially in tissue engineering requiring well-fabricated interfaces; thus, multimaterial bioprinting with controllable interfaces become more and more necessary [33, 34]. Due to the wide range of printing viscosity covered by the extrusion bioprinting method [35], it is expected to realize printing joints of materials with various attributes. However, the interface control in the current multimaterial switching process directly affects the printing accuracy and the actual interface effect, which is a bottleneck problem restricting the further development of the field. In this work, we presented the VCB technique that could fabricate the multimaterial tissue-like constructs with controllable interfaces. We designed the hardware and the software to overcome technical shortcomings the MPB approach brings.

We skillfully designed the printhead with the interlaced valve and the confluent nozzle. The novel valve could realize the rapid switching of materials through a straightforward rotary motion in a stable fluidic pressure. The viscoelasticity of biological materials has always been challenging to precise control. Polymer materials generally have non-negligible viscoelastic properties. The rotary valve isolates the precision interface assembling from the biomaterial inks' elastic potential energy in the cartridge. Besides, the rotary valve is cleverly designed so that the flow path of each material is completely free from contacting with others, which structurally avoids contamination between materials. The nozzle's unique shape allowed the material to be preassembled inside and to form a consecutive extrusion of multiple materials. Through the combination of rotary valves and air pressure, we could design and control a multimaterial interface in the form of boundary and suture. The design of this terminal, tiny, interlaced, and rotary valve provides an innovative solution to viscoelastic materials' control problem in bioprinting. The digital model and software workflow we developed were also the critical basis of the VCB method. The informative voxel digital model provided an extensible and flexible approach for data input and the digital process afterward. This software architecture is appropriate for all kinds of tissues modeling and bioprinting methods, including extrusion, inkjet, laser-assisted. We consider this digital model based on informative voxel an inevitable trend in biofabrication due to its applicability to tissues and organs' fine internal structure.

In contrast to the MPB method, the VCB method had significant advantages in interface accuracy, mechanical continuity, print efficiency, and printhead integration. From the printing tests we carried out, the VCB method alters the MPB method with improved functions. Compared to the high-resolution printing results published in [27], the VCB method achieved the control accuracy with inks by the design of the interlaced valve. We think that this method's most tremendous potential is to eliminate the multimaterial interface defects due to nozzle switching and improve printing efficiency, which is a highly potential solution for extrusion bioprinting in the future.

5. Conclusions

In this work, we present a VCB technique for multimaterial tissue-like constructs with controllable interfaces. By designing the innovative valve-based printhead and the voxelated digital model based on the Maxwell model analyzing, we accomplished the seamless rapid switching of multiple materials. Moreover, we compared this method with the primary method (MPB) quantitatively and comprehensively, indicating that the VCB method obtained greater mechanical strength (maximum tensile deformation increased by 44.37%) and higher printing efficiency (effective time ratio increased by 29.48%). As an exemplar, we fabricated a muscle-like stressed tissue with vascular tree and suture interface encapsulating C2C12 and HDFB cells, then we placed them in complete medium with continuous perfusion for 5 d. Our study suggests that the VCB method is sufficient to fabricate heterogeneous tissues with complex multimaterial interfaces.

Acknowledgments

The authors acknowledge funding support from the National Key Research and Development Project under Grant 2020YFB1313100, the Strategic Priority Research Program of the Chinese Academy of Sciences (XDA16020803), the National Natural Science Foundation of China (51875557), the Research Equipment Development Program of the Chinese Academy of Sciences (YZ201545, YJKYYQ20170042, YJKYYQ20190045), the National High Technology Research and Development Program of China (863 Program 2015AA020312) and The National Key Research and Development Program of China (2017YFC1104900), Foundation of State Key Laboratory of Robotics (2017-Z16).

ORCID iDs

Heran Wang https://orcid.org/0000-0003-3321-4438
Qi Gu https://orcid.org/0000-0001-9387-9525
Lianqing Liu https://orcid.org/0000-0002-2271-5870
Xiongfei Zheng https://orcid.org/0000-0001-9756-1119

References

[1] Sekine H, Shimizu T, Sakaguchi K, Dobashi I, Wada M, Yamato M, Kobayashi E, Umezu M and Okano T 2013 In vitro fabrication of functional three-dimensional tissues with perfusable blood vessels *Nat. Commun.* **4** 1399
[2] Murphy S V and Atala A 2014 3D bioprinting of tissues and organs *Nat. Biotechnol.* **32** 773–85
[3] Skylar-Scott M A, Uzel S G M, Nam L L, Ahrens J H, Truby R L, Damaraju S and Lewis J A 2019 Biomanufacturing of organ-specific tissues with high cellular density and embedded vascular channels *Sci. Adv.* **5** eaaw2459
[4] Faulkner-Jones A, Greenhough S, King J A, Gardner J, Courtney A and Shu W 2013 Development of a valve-based cell printer for the formation of human embryonic stem cell spheroid aggregates *Biofabrication* **5** 15013
[5] Faulkner-Jones A, Fyfe C, Cornelissen D-J, Gardner J, King J, Courtney A and Shu W 2015 Bioprinting of human pluripotent stem cells and their directed differentiation into hepatocyte-like cells for the generation of mini-livers in 3D *Biofabrication* **7** 44102
[6] Lin H, Zhang D, Alexander P G, Yang G, Tan J, Cheng A W-M and Tuan R S 2013 Application of visible light-based projection stereolithography for live cell-scaffold fabrication with designed architecture *Biomaterials* **34** 331–9
[7] Ma X *et al* 2016 Deterministically patterned biomimetic human iPSC-derived hepatic model via rapid 3D bioprinting *Proc. Natl Acad. Sci. USA* **113** 2206–11
[8] Koffler J *et al* 2019 Biomimetic 3D-printed scaffolds for spinal cord injury repair *Nat. Med.* **25** 263–9
[9] Miller J S *et al* 2012 Rapid casting of patterned vascular networks for perfusable engineered three-dimensional tissues *Nat. Mater.* **11** 768–74
[10] Tabriz A G, Hermida M A, Leslie N R and Shu W 2015 Three-dimensional bioprinting of complex cell laden alginate hydrogel structures *Biofabrication* **7** 45012
[11] Ouyang L, Yao R, Mao S, Chen X, Na J and Sun W 2015 Three-dimensional bioprinting of embryonic stem cells directs highly uniform embryoid body formation *Biofabrication* **7** 44101
[12] Ning E, Turnbull G, Clarke J, Picard F, Riches P, Vendrell M, Graham D, Wark A W, Faulds K and Shu W 2019 3D bioprinting of mature bacterial biofilms for antimicrobial resistance drug testing *Biofabrication* **11** 45018
[13] Grigoryan B *et al* 2019 Multivascular networks and functional intravascular topologies within biocompatible hydrogels *Science* **364** 458–64
[14] Derby B 2012 Printing and prototyping of tissues and scaffolds *Science* **338** 921–6
[15] Miri A K *et al* 2018 Microfluidics-Enabled Multimaterial Maskless Stereolithographic Bioprinting *Adv. Mater.* **30** e1800242
[16] Colosi C, Shin S R, Manoharan V, Massa S, Costantini M, Barbetta A, Dokmeci M R, Dentini M and Khademhosseini A 2016 Microfluidic Bioprinting of Heterogeneous 3D Tissue Constructs Using Low-Viscosity Bioink *Adv. Mater.* **28** 677–84
[17] Lee A, Hudson A R, Shiwarski D J, Tashman J W, Hinton T J, Yerneni S, Bliley J M, Campbell P G and Feinberg A W 2019 3D bioprinting of collagen to rebuild components of the human heart *Science* **365** 482–7
[18] Kolesky D B, Truby R L, Gladman A S, Busbee T A, Homan K A and Lewis J A 2014 3D bioprinting of vascularized, heterogeneous cell-laden tissue constructs *Adv. Mater.* **26** 3124–30
[19] Kang H-W, Lee S J, Ko I K, Kengla C, Yoo J J and Atala A 2016 A 3D bioprinting system to produce human-scale tissue constructs with structural integrity *Nat. Biotechnol.* **34** 312–9
[20] Schwartz J J and Boydston A J 2019 Multimaterial actinic spatial control 3D and 4D printing *Nat. Commun.* **10** 791
[21] Noor N, Shapira A, Edri R, Gal I, Wertheim L and Dvir T 2019 3D Printing of Personalized Thick and Perfusable Cardiac Patches and Hearts *Adv. Sci.* **6** 1900344
[22] Calejo I, Costa-Almeida R, Reis R L and Gomes M E 2019 Enthesis Tissue Engineering: Biological Requirements Meet at the Interface *Tissue Eng.* B **25** 330–56
[23] Li Y, Ortiz C and Boyce M C 2011 Stiffness and strength of suture joints in nature *Phys. Rev.* E **84** 62904
[24] Ober T J, Foresti D and Lewis J A 2015 Active mixing of complex fluids at the microscale *Proc. Natl Acad. Sci. USA* **112** 12293–8
[25] Hardin J O, Ober T J, Valentine A D and Lewis J A 2015 Microfluidic printheads for multimaterial 3D printing of viscoelastic Inks *Adv. Mater.* **27** 3279–84
[26] Liu W *et al* 2017 Rapid continuous multimaterial extrusion bioprinting *Adv. Mater.* **29** 1604630
[27] Skylar-Scott M A, Mueller J, Visser C W and Lewis J A 2019 Voxelated soft matter via multimaterial multinozzle 3D printing *Nature* **575** 330–5
[28] Bader C, Kolb D, Weaver J C, Sharma S, Hosny A, Costa J and Oxman N 2018 Making data matter: Voxel printing for the digital fabrication of data across scales and domains *Sci. Adv.* **4** eaas8652
[29] Groll J *et al* 2018 A definition of bioinks and their distinction from biomaterial inks *Biofabrication* **11** 13001
[30] Huang J, Fu H, Wang Z, Meng Q, Liu S, Wang H, Zheng X, Dai J and Zhang Z 2016 BMSCs-laden gelatin/sodium alginate/carboxymethyl chitosan hydrogel for 3D bioprinting *RSC Adv.* **6** 108423–30
[31] Du M, Chen B, Meng Q, Liu S, Zheng X, Zhang C, Wang H, Li H, Wang N and Dai J 2015 3D bioprinting of BMSC-laden methacrylamide gelatin scaffolds with CBD-BMP2-collagen microfibers *Biofabrication* **7** 44104
[32] Cellesi F, Tirelli N and Hubbell J A 2002 Materials for cell encapsulation via a new tandem approach combining reverse thermal gelation and covalent crosslinking *Macromol. Chem. Phys.* **203** 1466–72
[33] Liu Z, Meyers M A, Zhang Z and Ritchie R O 2017 Functional gradients and heterogeneities in biological materials: Design principles, functions, and bioinspired *Prog. Mater. Sci.* **88** 467–98
[34] Arrigoni C, Petta D, Bersini S, Mironov V, Candrian C and Moretti M 2019 Engineering complex muscle-tissue interfaces through microfabrication *Biofabrication* **11** 32004
[35] Sun W *et al* 2020 The bioprinting roadmap *Biofabrication* **12** 22002